Journal of Power Sources 196 (2011) 6781–6787

Contents lists available at ScienceDirect

Journal of Power Sources

journal homepage: www.elsevier.com/locate/jpowsour

Silver vanadium phosphorous oxide, $Ag_2VO_2PO_4$: *Chimie douce* preparation and resulting lithium cell electrochemistry

Young Jin Kim[a], Amy C. Marschilok[a,b], Kenneth J. Takeuchi[c], Esther S. Takeuchi[a,b,c,d,*]

[a] Department of Chemical and Biological Engineering, University at Buffalo (SUNY), Buffalo, NY 14260, USA
[b] Department of Electrical Engineering, University at Buffalo (SUNY), Buffalo, NY 14260, USA
[c] Department of Chemistry, University at Buffalo (SUNY), Buffalo, NY 14260, USA
[d] Department of Biomedical Engineering, University at Buffalo (SUNY), Buffalo, NY 14260, USA

ARTICLE INFO

Article history:
Received 13 July 2010
Received in revised form 4 October 2010
Accepted 18 October 2010
Available online 23 October 2010

Keywords:
Silver vanadium phosphorous oxide
Lithium battery
Implantable cardiac defibrillator
Chimie douce synthesis
Pulse discharge
Primary battery

ABSTRACT

Recently, we have shown silver vanadium phosphorous oxide ($Ag_2VO_2PO_4$, SVPO) to be a promising cathode material for lithium based batteries. Whereas the first reported preparation of SVPO employed an elevated pressure, hydrothermal approach, we report herein a novel ambient pressure synthesis method to prepare SVPO, where our *chimie douce* preparation is readily scalable and provides material with a smaller, more consistent particle size and higher surface area relative to SVPO prepared via the hydrothermal method. Lithium electrochemical cells utilizing SVPO cathodes made by our new process show improved power capability under constant current and pulse conditions over cells containing cathode from SVPO prepared via the hydrothermal method.

1. Introduction

The lithium/silver vanadium oxide (SVO, $Ag_2V_4O_{11}$) battery (Li/SVO) has been dominant as the power source for the implantable cardioverter defibrillator (ICD) for several decades [1–5]. The synthesis of SVO was reported in the 1930s [6,7], yet the successful implementation of SVO as a practical cathode material in a lithium battery occurred 50 years later, where a lithium anode battery with an SVO cathode was first utilized as an ICD power source [8,9]. A review of silver vanadium oxide and lithium battery applications appears in the literature [4].

There are three essential characteristics associated with SVO which are relevant to its use as a battery cathode material: (A) the electrochemical reduction of $Ag_2V_4O_{11}$ progresses with *in situ* formation of silver metal nanoparticles with an associated increase in cathode conductivity [10,11], (B) SVO exhibits significant decrease in (0 0 1) interlayer spacing corresponding to a 13% structural constriction of the vanadium-oxide layers as the electrochemical reduction progresses [12], (C) SVO can be prepared with a number of synthetic pathways, where resulting crystallinity, particle size and morphology can have significant impacts on its electrochemistry [4,13–18].

Recently, we identified silver vanadium phosphorous oxide ($Ag_2VO_2PO_4$, SVPO) to be a promising new cathode material for lithium based batteries, in particular for high power biomedical applications such as the implantable cardiac defibrillator. The first reported preparation of $Ag_2VO_2PO_4$ employed a hydrothermal synthesis method [19]. We reported the first electrochemical studies of SVPO, showing SVPO to be a suitable cathode material for high rate applications in lithium cells [20]. Consistent with our hypothesis based on the discharge mechanism of SVO, as electrochemical reduction of SVPO was initiated, *in situ* formation of silver nanoparticles in the cathode matrix was observed with an accompanying 15,000-fold increase in cathode conductivity [21]. However, counter to the structural collapse of SVO on discharge, SVPO showed no significant change in interlayer spacing [22]. This supported our expectation that the phosphorous oxide structure would add stability and rigidity to the SVPO framework.

In this study, we report a novel ambient pressure synthesis method for the preparation of $Ag_2VO_2PO_4$ (SVPO) with accompanying changes in morphology, particle size, and surface area over the previously reported preparation method. The synthesis method used for SVPO was adapted from a method we recently developed for preparation of silver hollandite, $Ag_{1.8}Mn_8O_{16}$ [23]. Electrochemical performances of SVPO prepared by the new synthesis method as well as the previously reported hydrothermal

* Corresponding author at: Department of Chemical and Biological Engineering, University at Buffalo (SUNY), 303 Furnas Hall, Buffalo, NY 14260, USA.
Tel.: +1 716 645 1185; fax: +1 716 645 3822.
E-mail address: et23@buffalo.edu (E.S. Takeuchi).

0378-7753/$ – see front matter © 2010 Elsevier B.V. All rights reserved.
doi:10.1016/j.jpowsour.2010.10.054

method are examined and compared. The results presented here further demonstrate the importance of the synthetic conditions and the impact of the preparation method on physical and electrochemical properties. This work takes significant steps toward the ability to tune electrochemical properties of cathode materials, including bi-metallic phosphates, by controlling not only molecular composition, but also physical properties.

2. Experimental

2.1. Material synthesis

Vanadium(V) oxide (V_2O_5), silver(I) oxide (Ag_2O), phosphoric acid (H_3PO_4, 85%) and de-ionized water were used as starting materials in the preparation of silver vanadium phosphorous oxide (SVPO). Silver vanadium phosphorous oxide (SVPO-H) was synthesized by a hydrothermal reaction according to a previously reported method [19].

Silver vanadium phosphorous oxide (SVPO-AP) was prepared using a novel reflux-based synthesis method where the reaction was conducted at atmospheric pressure at a temperature of ~100 °C with reaction times ranging from 24 to 96 h with a typical reaction time of 72 h. The synthesis method used for SVPO was adapted from a method we recently developed for preparation of silver hollandite, $Ag_{1.8}Mn_8O_{16}$ [23]. Notably, with the modified synthesis method, the starting material amounts could be readily scaled to increase the quantity of material produced. Further modification of SVPO-AP morphology and surface area was achieved by post synthesis heat treatment, where samples were heated at 500 °C for 24 h to produce SVPO-APS.

2.2. Material characterization

Scanning electron microscope (SEM) images were recorded using a Hitachi SU-70 field emitting scanning electron microscope. Powder X-ray diffraction (XRD) was performed using a Rigaku Ultima IV X-ray diffractometer with Cu Kα radiation with Bragg–Brentano geometry and a monochromator. An *in situ* high temperature stage was used for XRD measurements as a function of temperature. As-collected XRD patterns were analyzed using MDI JADE 8 software. Differential scanning calorimetry (DSC) was performed using a TA Instruments SDT Q600. Surface area of the samples was measured with a Micromeritics TriStar II using a multipoint BET (Brunauer, Emmett, and Teller) method. Particle size of the samples was determined with a Horiba LA-950V2 laser scattering particle size analyzer.

2.3. Electrochemical testing

Electrochemical tests were performed using coin-type experimental cells. Composite cathodes were prepared from a mixture of SVPO, graphite, and polytetrafluoroethylene compressed into a pellet. The anode was lithium metal foil, and the electrolyte was 1 M $LiAsF_6$ dissolved in 1:1 propylene carbonate:dimethoxyethane solution.

As-fabricated coin cells were discharged under constant current rates of C/10, C/50, C/100, and C/200 (equivalent current densities of 3.24, 0.65, 0.32, and 0.16 mA cm^{-2}). For the pre-discharge tests, cells were pre-discharged under a C/50 rate (0.65 mA cm^{-2}) to 1% depth of discharge with discharge continuing under C/10 (3.24 mA cm^{-2}). For the pulse discharge test, cells were discharged to 2 V under a background current of 0.19 mA cm^{-2} with 5 s pulses at alternating current densities (20, 30, and 40 mA cm^{-2}) applied every 8 h.

Galvanostatic intermittent titration technique (GITT) testing was done using a discharge current of 0.8 mA cm^{-2} applied for 2 h followed by open circuit for 20 h. This sequence was repeated until the cells were discharged to 4 electron equivalents. All electrochemical tests were performed at 37 °C using a Maccor Series 4000 battery tester.

3. Results and discussion

3.1. Novel synthesis and characterization of $Ag_2VO_2PO_4$ (SVPO-H and SVPO-AP)

Previous reports regarding the preparation of $Ag_2VO_2PO_4$, SVPO utilized hydrothermal reaction conditions, generating SVPO-H material at a reaction temperature of 230 °C and elevated pressure. In this study, we report a novel approach for synthesis where SVPO was prepared under ambient pressure conditions, generating SVPO-AP at a temperature of ~100 °C. Ambient pressure reaction conditions provide a facile method for material preparation and are readily scalable with only simple reaction equipment needed.

The prepared SVPO samples were characterized using X-ray powder diffraction. The XRD patterns of SVPO samples compared well with the previously reported reference data [ref: JCPDS#07-3580, PDF#97-007-3580, FIZ#73580], (Fig. 1). For the SVPO-H material it should be noted that the intensity of the peak at $2\theta = 28.703°$ is higher relative to peaks at $2\theta = 31.742°$, 31.911°, 34.904°, and 34.985° than for material prepared at ambient pressure or for the reference pattern. SVPO-H has large acicular particles that can show preferred orientation due to the high aspect ratio of the particles [24].

Thermal analysis was utilized to determine if other phases of materials were present. Differential scanning calorimetry (DSC) of all SVPO materials displayed a single endotherm at ~540 °C without additional peaks. These results further support the XRD observations regarding the presence of one single phase in each material sample.

SEM images reveal the morphology and particle size of the samples (Fig. 2). SVPO-H is comprised of stacked rod-like structures with some small particles distributed on the surface of the rods. The large rods had an aspect ratio of ~10 with typical width dimensions of ~7 μm and length dimensions of ~75 μm. The smaller surface adhered particles had typical dimensions of 0.5–3 μm. The morphology and size of the SVPO-AP was quite distinct from the material prepared by the hydrothermal pathway (SVPO-H). In the SVPO-AP material, the larger rod shaped structures were absent and instead small more uniformly sized granular particles were observed with dimensions in the 0.2–0.6 μm range.

Sample particle size was quantitatively determined by laser light scattering methodology. The particle size distributions of the samples are shown (Fig. 3). The SVPO-H had three local maxima around 0.7, 5 and 15 μm with a shoulder near 70 μm. This wide distribution of these major peaks is consistent with the high aspect ratio rod shaped particles. A secondary peak around 0.7 μm is consistent with the small particles observed on the surface of the larger rods. The SVPO-AP sample had a distribution centered at around 0.5 μm with a small shoulder at 3 μm illustrating both a smaller and more consistent particle size range than the hydrothermal material. Results from the laser scattering particle size distribution analysis displayed good correspondence with the SEM image analysis of the SVPO samples.

Surface area of the SVPO-H material was determined using nitrogen adsorption by BET. The surface area values of the SVPO-H were on average 0.29 $m^2\ g^{-1}$, with a 95% confidence interval of 0.25–0.33 $m^2\ g^{-1}$ while SVPO-AP was 4.11 $m^2\ g^{-1}$ on average with a 95% confidence interval of 3.61–4.61 $m^2\ g^{-1}$. Thus, the surface area

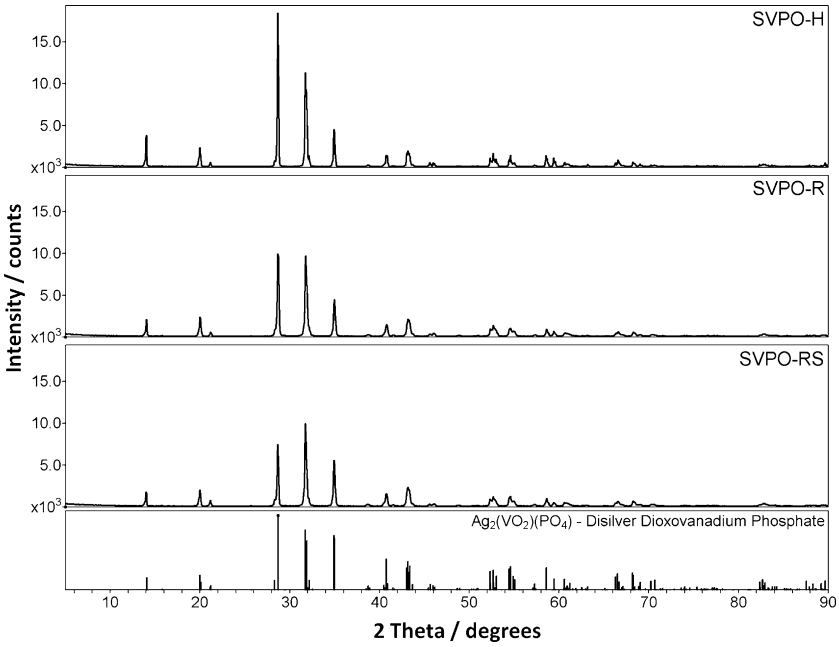

Fig. 1. XRD pattern of hydrothermal (SVPO-H), ambient pressure (SVPO-AP) and sintered (SVPO-APS) SVPO materials.

of SVPO-AP was more than 10-fold larger than that of the SVPO-H sample. This difference in measured surface area is consistent with the observed changes in morphology and particle size of the SVPO samples prepared by the two synthetic methods.

Differences in particle size and surface area of the SVPO-H and SVPO-AP samples are attributed to differences in the synthesis conditions. Relative to the SVPO-H material, the SVPO-AP material was synthesized under considerably less strenuous conditions, with less than one half of the reaction temperature, at ambient pressure rather than elevated pressure, and typically for shorter reaction times. Thus, the opportunity for growth of large crystals for the SVPO-AP material was significantly reduced compared to the SVPO-H material.

3.2. Post heat treatment (sintering) of SVPO-AP to form SVPO-APS

As there was a significant difference in surface area of the SVPO-AP and SVPO-H, sintering was investigated to modify the surface area of SVPO-AP. The objective of this study was to align the surface area values of the as-prepared hydrothermal material (SVPO-H) and the sintered ambient pressure prepared material (SVPO-APS) to evaluate the effects of particle size and morphology on the electrochemical behavior of the SVPO materials without a large surface area effect.

In order to identify appropriate sintering conditions, a detailed examination of the changes in SVPO with temperature increase was done using *in situ* XRD measurements. A sample of SVPO-

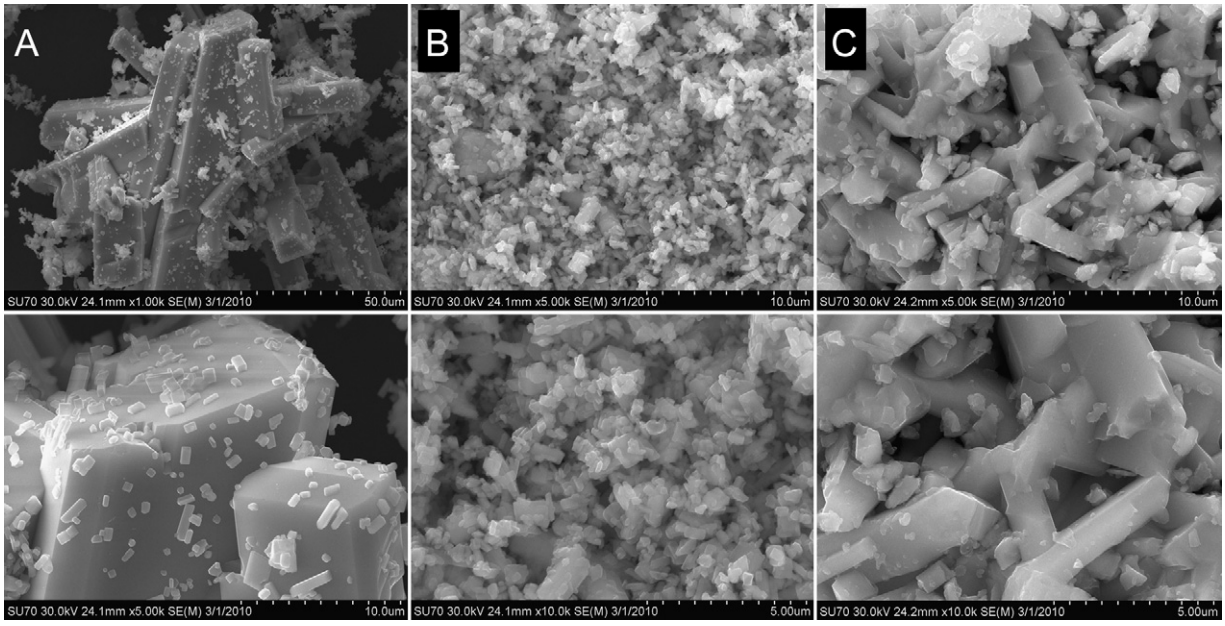

Fig. 2. SEM images of (a) SVPO-H 1000X and 5000X, (b) SVPO-AP 5000X and 10,000X, and (c) SVPO-APS 5000X and 10,000X.

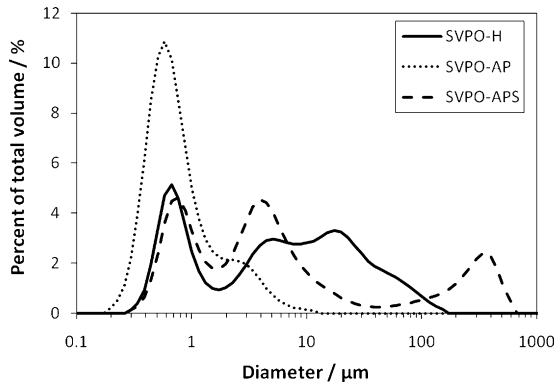

Fig. 3. Particle size distribution of SVPO-H, SVPO-AP and SVPO-APS materials.

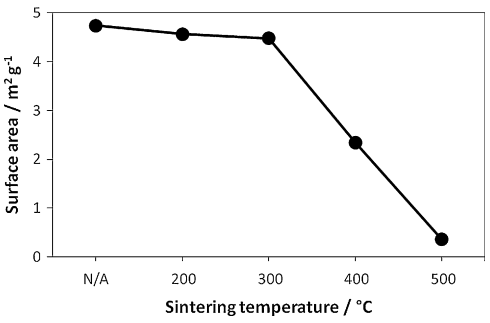

Fig. 5. Surface area change of SVPO-AP during the post heat treatment.

AP was heated stepwise at 200, 300, 400, and 500 °C, and the diffraction patterns at each temperature were recorded (Fig. 4). The diffraction pattern shifted to lower 2θ angles with increases in temperature. This phenomenon is attributed to the heat expansion of the crystal structure of SVPO where an increase in the lattice spacing of the unit cell results in peak shift to lower 2θ in the diffraction pattern, as expressed by Bragg's law [25]. Lattice expansion with increasing temperature has been observed previously in other materials [26–28]. In addition, peak separation was observed at higher temperatures, indicating an anisotropic expansion for SVPO. Anisotropic thermal expansion has been previously reported for other materials [29].

At 400 and 500 °C, several peaks at $2\theta = \sim 19.9°$, 21.2°, 31.7°, and 34.9° showed peak separation, while the peaks at $2\theta = \sim 14.1°$ and 28.7° did not separate. The peaks which separated at high temperature were assigned to two or more overlapping peaks representing different reflection planes in a narrow 2θ range at room temperature. Since the SVPO material has a monoclinic cell structure, the extent of d-spacing increase due to the lattice expansion should not be the same for different reflection planes. For example, the peak at $2\theta = \sim 19.9°$ consists of two peaks representing (−2 0 1) and (2 0 1) planes. Those planes had similar d-spacing of 4.439 Å, with one peak visible at room temperature. At 500 °C, the peak separated into two peaks and the d-spacing for two planes was increased to 4.516 and 4.452 for the (−2 0 1) and (2 0 1) planes, respectively.

After cooling to room temperature, the XRD pattern of the heat treated material returned to the same pattern as before sintering, confirming that the SVPO material showed good thermal stability and did not decompose. Sintering the SVPO material allowed modification of the physical properties of the material while maintaining the sample chemistry and crystal structure. Based on the *in situ* XRD heating study 500 °C was identified to be an appropriate temperature for the sintering treatment.

A larger sample of SVPO-AP was subjected to heat treatment and then characterized. The heat treated SVPO-AP is designated as SVPO-APS. Physical property changes are observed post heat treatment. The material shows a decrease in BET surface area as a function of temperature with a large decrease noted for samples sintered at or above 300 °C (Fig. 5). After sintering at 500 °C, the sample surface area reached 0.34 $m^2 g^{-1}$, which was similar to typical surface area of the SVPO-H material. A significant morphology change could also be observed in the sample sintered at 500 °C (Fig. 2c). The typically smaller particles of SVPO-AP were agglomerated and appeared to be fused forming larger particles.

The particle size distribution of the sintered material showed an interesting trend (Fig. 3). While two major peaks around 0.8 and 4 μm corresponded well with the SEM analysis showing larger fused particles, there was another peak apparent above 300 μm. This peak is consistent with a large fused structure for the sintered material. During the sintering, it appears that the small particles of the SVPO-AP material agglomerated and fused into larger particles. The fused particles then merged to make an even larger fused structure. The larger fused structures did not readily disperse as sonication conducted as part of the particle size determination did not disrupt the material and return it to individual particles.

Crystallite size analysis was performed using XRD data, for the SVPO-H, SVPO-AP, and SVPO-APS materials. Two diffraction peaks at $2\theta = 14.046°$ and 28.703°, representing the (0 0 1) and (4 0 0) planes respectively, were chosen for the analysis. The sample crystallite size for each direction was calculated by the Scherrer equation. There was a clear difference in the crystallite sizes for the three SVPO types (Fig. 6). In both crystallographic directions, the ambient pressure material (SVPO-AP) showed the smallest crystallite size, the hydrothermal material (SVPO-H) had the largest, and the sintered material (SVPO-APS) had intermediate values. These results correspond to the characterization results from the SEM and particle size analysis. The SVPO-H and SVPO-APS showed crystallite sizes larger than the SVPO-AP material along the *a*-axis direction, as

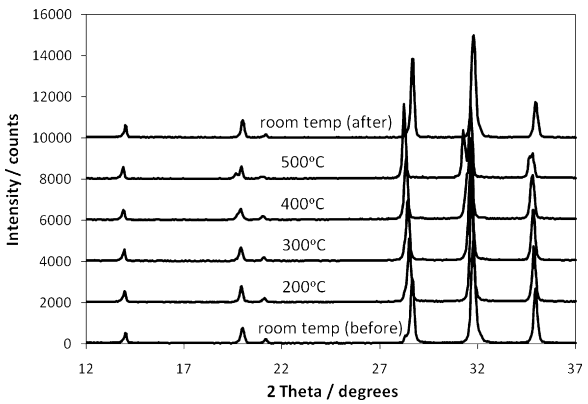

Fig. 4. XRD patterns of SVPO-AP at different temperatures.

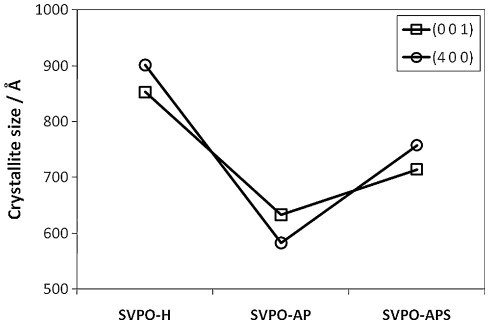

Fig. 6. Crystallite size of SVPO-H, SVPO-AP and SVPO-APS materials.

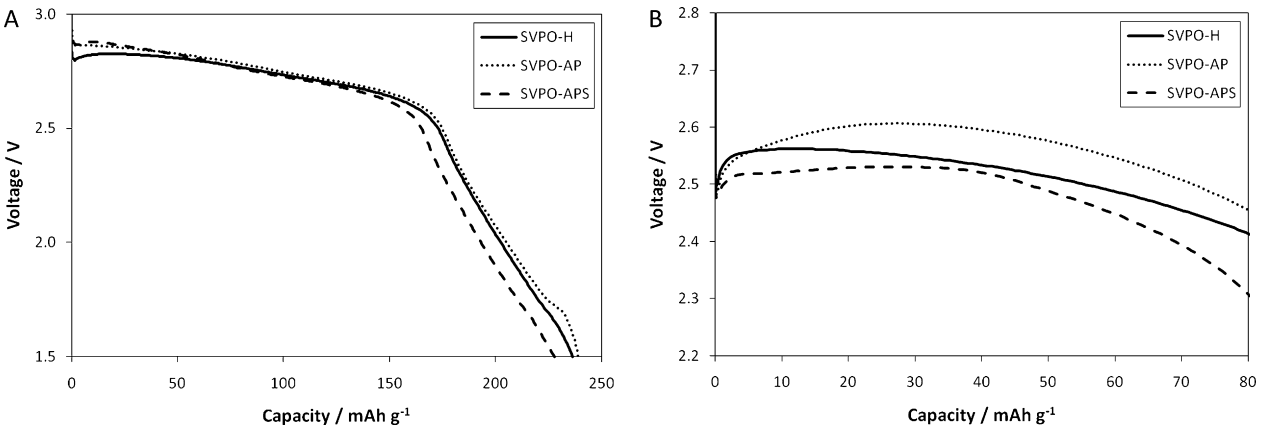

Fig. 7. Constant discharge curve of Li/SVPO (SVPO-H, SVPO-AP and SVPO-APS) cells at (a) C/100 and (B) C/10 rates.

represented by the (4 0 0) plane, than along the *c*-axis direction, as represented by the (0 0 1) plane. Analysis of the XRD data for SVPO shows that the VOPO layers extend parallel to the (0 0 1) plane [20]. The data suggest that the long dimension of the acicular particles for SVPO-H and SVPO-APS is along the *c*-axis.

3.3. Electrochemical evaluation

To investigate the electrochemical performance of the three SVPO materials, cathodes were fabricated and incorporated into test cells utilizing lithium anodes. It was anticipated that even though the chemical structure and composition of the three SVPO samples were the same, the difference in physical properties would influence their electrochemical performance.

Constant current discharge tests were conducted at discharge rates of C/10 (3.24 mA cm^{-2}), C/50 (0.65 mA cm^{-2}), C/100 (0.32 mA cm^{-2}), and C/200 (0.16 mA cm^{-2}), where C/10 and C/100 are shown (Fig. 7). If a lower discharge rate was used (C/50 and below), the test cells with SVPO-AP and SVPO-H showed similar voltages and delivered similar total capacities. At the highest discharge rate used (C/10) the cells using SVPO-AP showed higher voltage, in the middle of life, than the cells using SVPO-H. However, the SVPO-AP material delivered slightly less capacity to 2.0 V and 1.5 V limits. The SVPO-APS cells displayed the largest variation in performance and generally delivered less total capacity than the SVPO-H and SVPO-AP cells.

Previously, a significant increase in cathode conductivity was noted on initiation of discharge of SVPO cells [21]. Therefore, the effect of pre-discharge of the cells was investigated as it was anticipated that a conductive network would be formed within the cathode structure. Groups of experimental cells containing SVPO-H and SVPO-AP were pre-discharged at a C/50 rate to 1% depth of discharge (DOD) and then discharge was continued under a C/10 rate. Pre-discharge of the cells mitigates the initial voltage drop observed as the load is first applied consistent with the formation of a more conductive cathode during the predischarge step (Fig. 8). Pre-discharge did not influence the total delivered capacity of the test cells and as expected the initial voltage of the SVPO-AP cells was higher than that of the SVPO-H cells.

To investigate cell behavior under conditions that are more consistent with a high power biomedical application such as the ICD, test cells were discharged with intermittent pulses at alternating current densities (Fig. 9). Starting from an initial voltage of ~3.5 V, the cells reached a loaded potential of 2 V at a capacity of ~200 mAh g^{-1}. Similar to the results of the constant discharge tests, the total capacity delivered to 2 V for the SVPO-H and SVPO-AP cells was similar. The sintered SVPO-APS cells generally displayed lower total capacity.

Resistance at each pulse was calculated using Ohm's law and the point of maximum voltage drop (Fig. 10). Cells containing SVPO-AP showed lower resistance, while those containing SVPO-APS and SVPO-H showed similar resistances. The ohmic and polarization contributions to the voltage drop were determined by analysis of the pulse data where the ohmic contribution was assigned as the initial rapid voltage drop on application of the pulse current. Interestingly, differences in the ohmic resistances of the SVPO materials were more significant than differences in the polarization resistance, where a representative example for one pulse is shown

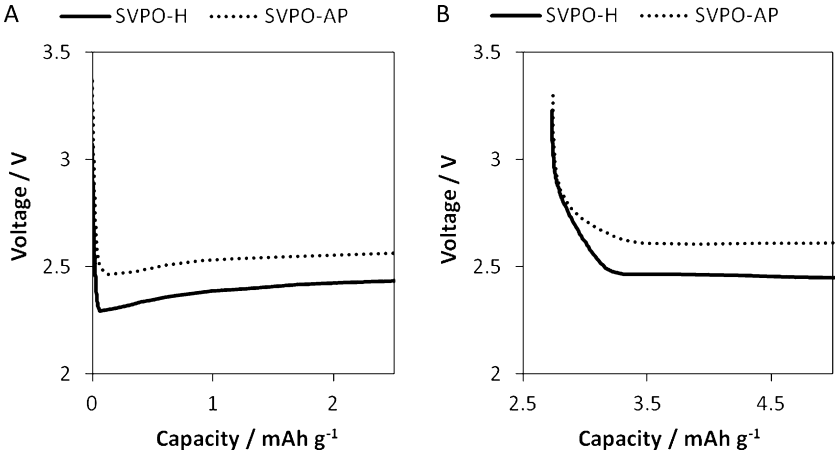

Fig. 8. Initial discharge curve of Li/SVPO cells (SVPO-H and SVPO-AP) (a) without pre-discharge and (b) after pre-discharge.

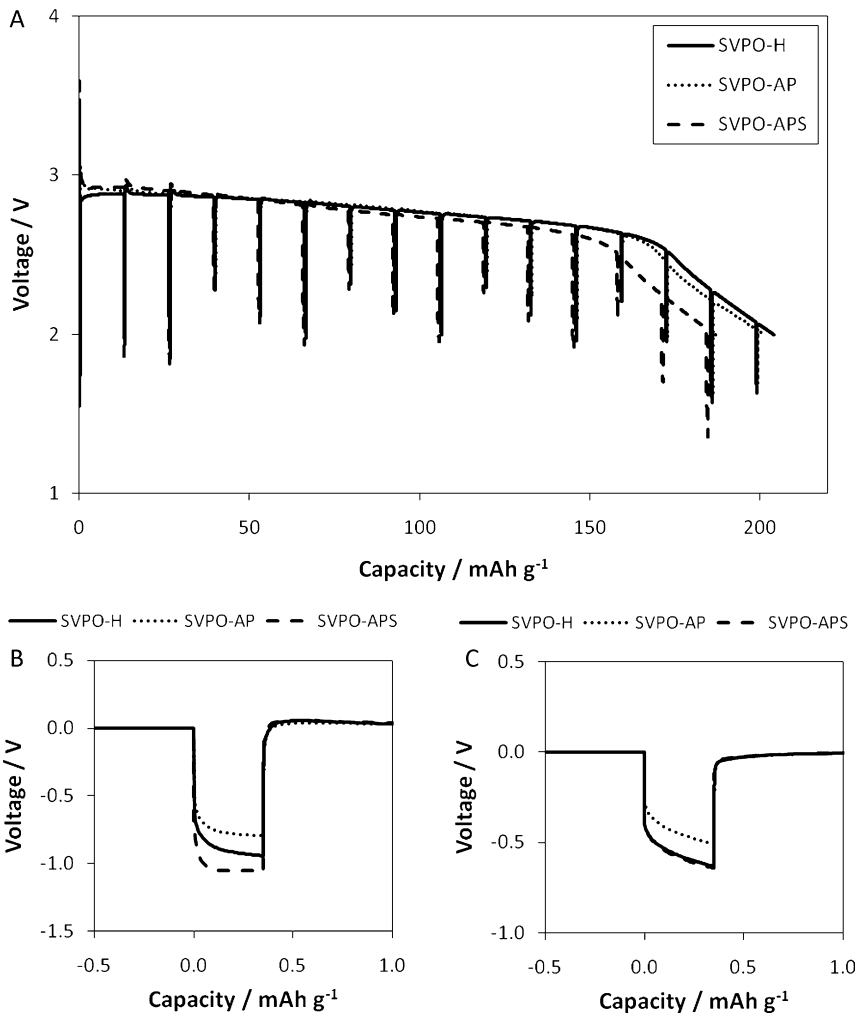

Fig. 9. (a) Pulse discharge curve of Li/SVPO cells (SVPO-H, SVPO-AP and SVPO-APS): magnification of 30 mA cm^{-2} pulses at (b) ~13 mAh g^{-1} and (c) ~92 mAh g^{-1}.

(Fig. 11). Less voltage drop and lower resistance of the cells using the SVPO-AP cathodes can provide better power capability for high current load applications. Results of the discharge tests affirm that differences in sample surface area and/or particle size can affect the discharge behavior of batteries under high rate pulse conditions. However, as expected, there was little influence on the intrinsic capacity of the material.

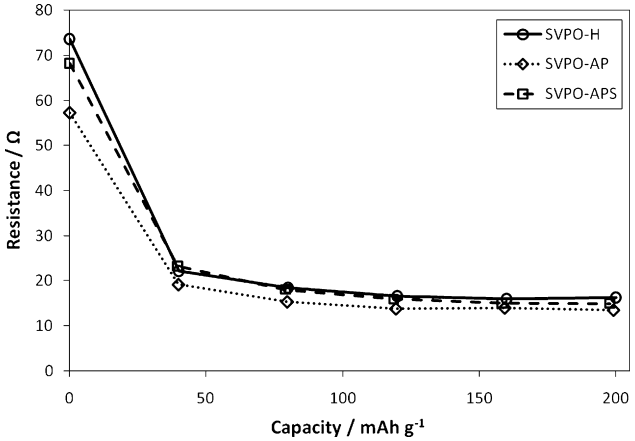

Fig. 10. Cell resistances for Li/SVPO (SVPO-H, SVPO-AP and SVPO-APS) cells under 20 mA cm^{-2} pulses.

Galvanostatic intermittent titration technique (GITT) was utilized to further investigate the polarization of the SVPO cathodes. The overall trend of the cathode polarization can be observed as a function of discharge (Fig. 12). Consistent with our analysis of the pulse discharge data discussed above, polarization differences of cell prepared with SVPO-AP, SVPO-APS, and SVPO-H cathode materials under GITT test were not significant. Notably, over the course of the discharge curve, the polarization is initially higher and decreases as the cells discharge. A significant change in the

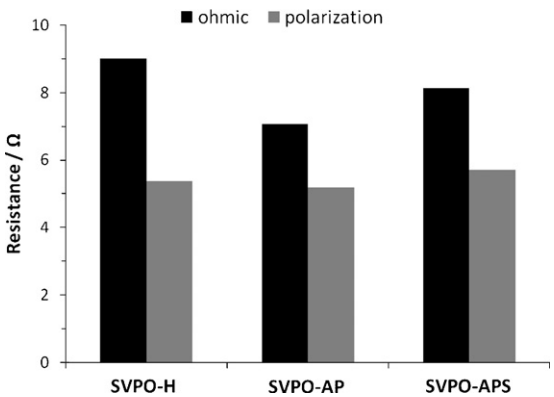

Fig. 11. Ohmic and polarization contributions to cell resistance for 40 mA cm^{-2} pulse at ~100 mAh g^{-1}.

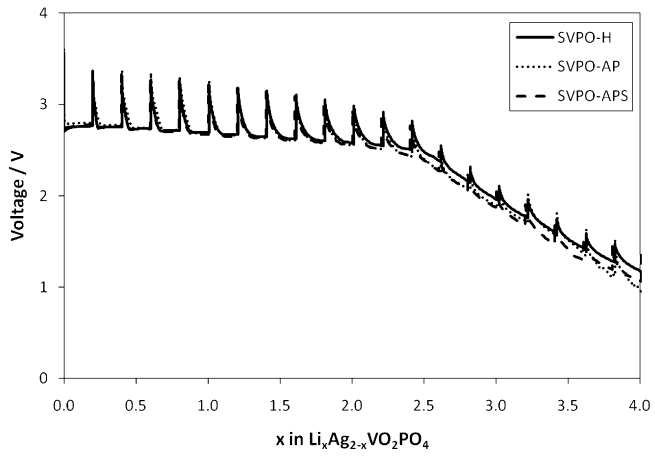

Fig. 12. GITT polarization curves of Li/SVPO (SVPO-H, SVPO-AP and SVPO-APS) cells.

polarization occurs after 2.4 electrons have been incorporated by the cathode, at around 2.6 V. This observation is consistent with two different reaction zones in the discharge behavior, before and after $x \sim 2.4$ in $Li_xAg_{2-x}VO_2PO_4$. From our previous study on SVPO material [21], it was found that in the initial region of discharge reduction of Ag^+ to Ag^0 is the dominant process with some reduction of V^{5+} occurring in parallel (up to $x = 2.4$). After $x \sim 2.4$, the Ag^+ reduction is largely complete and the predominant reduction process is reduction of V^{5+} to V^{4+}. The change in mechanism with the progression of discharge is consistent with the GITT results, where more polarization is observed in the early stages of the discharge during the Ag^+ reduction process and less polarization is observed when the dominant process shifts to vanadium reduction with lithium insertion.

4. Summary

A novel synthesis of silver vanadium phosphorous oxide, $Ag_2VO_2PO_4$, is reported. Our synthetic approach is readily scalable and provides material with a smaller, more consistent particle size and higher surface area. Cells utilizing SVPO cathodes made by the new process show improved power capability under constant current and pulse conditions. The results presented here further demonstrate the importance of the synthetic conditions and the impact of the preparation method on physical and electrochemical properties. This work establishes new paradigms for the tuning of electrochemical properties of cathode materials, including bi-metallic phosphates, by controlling not only elemental composition, but also physical properties of the materials.

Acknowledgements

This project was supported by the University at Buffalo (SUNY) and the National Institutes of Health under Grant 1R01HL093044-01A1 from the National Heart, Lung, and Blood Institute. The authors thank Chia-Ying Lee for scanning electron microscopy.

References

[1] E.S. Takeuchi, W.C. Thiebolt III, J. Electrochem. Soc. 135 (1988) 2691–2694.
[2] R.A. Leising, W.C. Thiebolt III, E.S. Takeuchi, Inorg. Chem. 33 (1994) 5733–5740.
[3] E.S. Takeuchi, W.D.K. Clark, in: N.A.M. Estes, A.S. Manolis, P. Wang (Eds.), Implantable Cardioverter-Defibrillators: A Comprehensive Textbook, Marcel Dekker, New York, 1994, p. pp. 123.
[4] K.J. Takeuchi, A.C. Marschilok, S.M. Davis, R.A. Leising, E.S. Takeuchi, Coord. Chem. Rev. 219–221 (2001) 283–310.
[5] K.J. Takeuchi, A.C. Marschilok, E.S. Takeuchi, in: A.S. Tracey, G.R. Willsky, E.S. Takeuchi (Eds.), Vanadium: Chemistry, Biochemistry, Pharmacology and Practical Applications, Taylor and Francis, New York, 2007.
[6] H.T.S. Britton, R.A. Robinson, J. Chem. Soc. (1930) 2328–2343.
[7] H.T.S. Britton, R.A. Robinson, J. Chem. Soc. (1933) 512–517.
[8] C.F. Holmes, P.P. Keister, E.S. Takeuchi, Prog. Batteries Solar Cells 6 (1987) 64–66.
[9] E.S. Takeuchi, P. Piliero, J. Power Sources 21 (1987) 133–141.
[10] N.R. Gleason, R.A. Leising, M. Palazzo, E.S. Takeuchi, K.J. Takeuchi, 208th Meeting of the Electrochemical Society. Session D2 – Rechargeable Lithium and Lithium-Ion Batteries – Battery/Energy Technology, Friday, October 1, 2005.
[11] N.D. Leifer, A. Colon, K. Martocci, S.G. Greenbaum, F.M. Alamgir, T.B. Reddy, N.R. Gleason, R.A. Leising, E.S. Takeuchi, J. Electrochem. Soc. 154 (2007) A500–A506.
[12] R.A. Leising, W.C. Thiebolt, E.S. Takeuchi, Inorg. Chem. 33 (1994) 5733–5740.
[13] K.J. Takeuchi, A.C. Marschilok, E.S. Takeuchi, Preparation, characterization, and battery applications of silver vanadium oxide materials, in: A.S. Tracey, G.R. Willsky, E.S. Takeuchi (Eds.), Vanadium: Chemistry, Biochemistry, Pharmacology and Practical Applications, Taylor and Francis, New York, 2007.
[14] T.A. Albrecht, F. Sauvage, V. Bodenez, J.-M. Tarascon, K.R. Poeppelmeier, Chem. Mater. 21 (2009) 3017–3020.
[15] F. Sauvage, V. Bodenez, J.-M. Tarascon, K.R. Poeppelmeier, J. Am. Chem. Soc. 132 (2010) 6778–6782.
[16] S. Zhang, W. Li, C. Li, J. Chen, J. Phys. Chem. B 110 (2006) 24855–24863.
[17] X. Cao, L. Xie, H. Zhan, Y. Zhou, Inorg. Mater. 44 (2008) 886–889.
[18] F. Sauvage, V. Bodenez, H. Vezin, M. Morcrette, J.M. Tarascon, K.R. Poeppelmeier, J. Power Sources 195 (2010) 1195–1201.
[19] H.Y. Kang, S.L. Wang, P.P. Tsai, K.H. Lii, J. Chem. Soc. Dalton Trans. (1993) 1525–1528.
[20] A.C. Marschilok, K.J. Takeuchi, E.S. Takeuchi, Electrochem. Solid-State Lett. 12 (2008) A5–A9.
[21] E.S. Takeuchi, A.C. Marschilok, K. Tanzil, E.S. Kozarsky, S. Zhu, K.J. Takeuchi, Chem. Mater. (2009).
[22] A.C. Marschilok, E.S. Kozarsky, K. Tanzil, S. Zhu, K.J. Takeuchi, E.S. Takeuchi, J. Power Sources 195 (2010) 6829–6846.
[23] S. Zhu, A.C. Marschilok, C.-Y. Lee, E.S. Takeuchi, K.J. Takeuchi, Electrochem. Solid-State Lett. 13 (2010) A98–A100.
[24] B.B. He, Two-dimensional X-ray Diffraction, Wiley, Hoboken, NJ, 2009.
[25] W.L. Bragg, Proc. Cambridge Philos. Soc. 17 (1913) 43–57.
[26] R. Banerjee, E.A. Sperling, G.B. Thompson, H.L. Fraser, S. Bose, P. Ayyub, Appl. Phys. Lett. 82 (2003) 4250–4252.
[27] R. Lamber, S. Wetjen, N.I. Jaeger, Phys. Rev. B: Condens. Matter 51 (1995) 10968–10971.
[28] P. Singh, A. Kumar, A. Kaushal, D. Kaur, A. Pandey, R.N. Goyal, Bull. Mater. Sci. 31 (2008) 573–577.
[29] S.N. Achary, S.J. Patwe, M.D. Mathews, A.K. Tyagi, J. Phys. Chem. Solids 67 (2006) 774–781.